Mutations Designed To Modify the Environment of the Primary Electron Donor of the Reaction Center from *Rhodobacter sphaeroides*: Phenylalanine to Leucine at L167 and Histidine to Phenylalanine at L168†

H. A. Murchison, R. G. Alden, J. P. Allen, J. M. Peloquin, A. K. W. Taguchi, N. W. Woodbury, and J. C. Williams*

Department of Chemistry and Biochemistry and Center for the Study of Early Events in Photosynthesis, Arizona State University, Tempe, Arizona 85287-1604

Received November 11, 1992; Revised Manuscript Received January 27, 1993

ABSTRACT: Two mutations, L168 His to Phe and L167 Phe to Leu, were made in residues near the primary electron donor, a bacteriochlorophyll dimer, of the reaction center from *Rhodobacter sphaeroides*. Blue shifts of 10–15 nm in the 865-nm band of the donor were observed in the optical absorption spectra of both of the mutant reaction centers. The rate of initial electron transfer was determined by measurement of the kinetics of the decay of the excited state of the donor, and the rate of charge recombination was determined by measurement of the recovery of the bleaching of the donor. The initial electron transfer time constant and the charge recombination time constant were determined to be 3.6 ps and 220 ms, respectively, in the L168 His to Phe mutant and 5.0 ps and 85 ms in the L167 Phe to Leu mutant, compared to 3.8 ps and 100 ms measured for the wild type. The oxidation potential of the donor measured by oxidation–reduction titrations was found to decrease by 80 mV in the L168 His to Phe mutant and increase by 25 mV in the L167 Phe to Leu mutant. Time-resolved fluorescence decay measurements indicated that the change in the oxidation potential of the donor in the L168 His to Phe mutant resulted in a change in the energies of the charge-separated states. The results show that an increase in the driving force does not increase the rate of the initial electron transfer reaction. The mutation L168 His to Phe causes the loss of a hydrogen bond to a ring I acetyl group of the bacteriochlorophyll dimer, demonstrating that the midpoint potential of the primary electron donor in bacterial reaction centers can be correlated with hydrogen-bonding interactions with the surrounding protein.

The bacterial reaction center is a membrane-bound pigment–protein complex that is responsible for the primary photochemical events in photosynthesis. The absorption spectra and energy levels of the bacteriochlorophylls (Bchls)[1] in the reaction center are modified by interactions of the Bchls with the protein [reviewed in Scheer (1991)]. This modification includes specific interactions such as hydrogen bonding between the Bchls and the protein as well as more general effects such as the local dielectric constant produced by the protein surrounding the Bchls. We are investigating the interactions of the protein and the Bchls by altering amino acid residues that are in contact with the primary electron donor.

The three dimensional structures of reaction centers from two bacterial species, *Rhodopseudomonas viridis* (Michel et al., 1986) and *Rhodobacter sphaeroides* (Yeates et al., 1988; El-Kabbani et al., 1991), have been determined by X-ray diffraction. The wild-type *Rb. sphaeroides* 2.4.1. reaction center is composed of three protein subunits, L, M, and H, and several cofactors, a Bchl *a* dimer (P), two monomer Bchl *a* molecules (B_A and B_B), two bacteriopheophytin *a* molecules (H_A and H_B), two ubiquinones (Q_A and Q_B), a carotenoid, and a non-heme iron. Both the L and M core subunits as well as the A and B branches of cofactors are related by an approximate C2 rotational axis. Upon absorption of light, the lowest excited singlet state of the electron donor, P*, is formed. An electron is transferred from P* to H_A in approximately 3.5 ps, and subsequently the electron is transferred to Q_A in 200 ps and Q_B in 200 μs [see reviews by Kirmaier and Holten (1987) and Feher et al. (1989)].

Several mutants of reaction centers in both *Rb. sphaeroides* and *Rhodobacter capsulatus* have been reported in which the putative addition of a hydrogen bond is correlated with an increase in the oxidation–reduction midpoint potential of the primary electron donor. Two mutations in *Rb. sphaeroides* reaction centers that were designed to introduce hydrogen bonds to the ring V keto groups of the dimer, L131 Leu to His and M160 Leu to His, showed increases of 80 and 55 mV, respectively, in the P/P^+ midpoint potentials relative to that of wild type (Williams et al., 1992a). A *Rb. capsulatus* mutant, *syml*, has been reported in which a portion of the M subunit (residues M187–M203) was replaced with the symmetry-related L subunit sequences (Woodbury et al., 1990; Taguchi et al., 1992). Isolated *syml* reaction centers have a P/P^+ midpoint potential higher than that of wild type by at least 100 mV (Stocker et al., 1992). The changes to the M subunit in *syml* include the mutation M195 Phe to His, which appears to be principally responsible for the elevated donor midpoint potential since single-site mutations at M195 in *Rb. capsulatus* (Stocker et al., 1992) and at the equivalent

† This work was supported by Grants GM41300 and GM45902 from the NIH, Grants DMB89-177729 and DMB91-58251 from the NSF, and Postdoctoral Fellowship in Plant Biology DIR-9104322 from the NSF. Instrumentation was purchased with funds from NSF Grant BBS-88-04992 and DOE Grants DE-FG05-88ER75443 and DE-FG05-87ER75361. This is publication no. 132 from the Arizona State University Center for the Study of Early Events in Photosynthesis. The Center is funded by U.S. Department of Energy Grant DE-FG02-88ER13969 as part of the USDA/DOE/NSF Plant Science Centers Program.

[1] Abbreviations: Bchl, bacteriochlorophyll; P, Bchl dimer, B, Bchl monomer, H, bacteriopheophytin monomer; Q, quinone; EDTA, ethylenediaminetetraacetic acid; Tris, tris(hydroxymethyl)aminomethane; TLE, 15 mM Tris-HCl, pH 8.0, 0.025% lauryldimethylamine *N*-oxide, and 1 mM EDTA buffer.

0006-2960/93/0432-3498$04.00/0

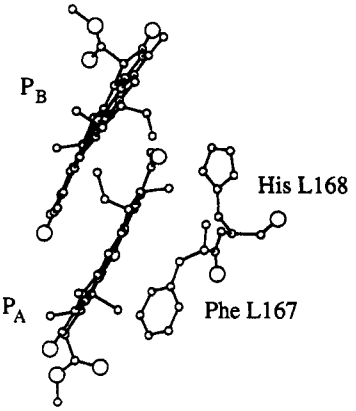

FIGURE 1: Dimer Bchls (P_A and P_B) with residues L167 and L168 of the *Rb. sphaeroides* wild-type reaction center structure. Residue L168 comes within 4 Å of the P_A ring I acetyl group oxygen. The view is approximately down the C2 axis of symmetry. Coordinates are from the Brookhaven National Laboratory Protein Data Bank, file 4RCR (Allen et al., 1987; Yeates et al., 1988).

site, M197, in *Rb. sphaeroides* (Murchison et al., 1991) result in similar increases in the donor midpoint potential. On the basis of the *Rb. sphaeroides* structure (Yeates et al., 1988; El-Kabbani et al., 1991), the mutation M197 Phe to His could add a hydrogen bond to the ring I acetyl group of the B-side Bchl of the dimer.

The interactions between amino acid residues and the primary electron donor have been further explored by studying the effects of two mutations in the L subunit of *Rb. sphaeroides*. In the HF(L168) mutant, the histidine at residue L168 was replaced with phenylalanine, and in the FL(L167) mutant, the phenylalanine at residue L167 was replaced with leucine (Figure 1). The L168 His to Phe mutation removes a hydrogen-bonding group from near the ring I acetyl group of the dimer, while the L167 Phe to Leu mutation is a more general change in the properties of a residue contacting the dimer. A comparison of these two mutations should facilitate the identification of characteristics of the donor that are specifically associated with hydrogen bonding. In this paper we report the oxidation midpoint potential of the donor, the spectral features, and the electron transfer properties of isolated reaction centers containing these mutations.

MATERIALS AND METHODS

Mutagenesis. The mutants were constructed using site-directed mutagenesis techniques described in detail elsewhere (Paddock et al., 1989). A portion of the L gene was cloned into the phage M13mp19 and the changes Phe (TTC) to Leu (CTC) at residue L167 and His (CAC) to Phe (TTC) at residue L168 were made by oligonucleotide-directed in vitro mutagenesis (Amersham). Phage DNA from plaques was screened by single-lane sequencing, followed by complete sequencing of the ~440 base pair *Asp*718I–*Sal*I fragment of selected clones. This fragment was subcloned into a plasmid containing the *puf* operon. Plasmids containing the mutations were transformed into the *Escherichia coli* strain S17-1 (Simon et al., 1983) and mated into the ΔLM1.1 deletion strain of *Rb. sphaeroides* 2.4.1 (Paddock et al., 1989).

Bacterial Growth and Reaction Center Isolation. Mutant strains were grown semiaerobically in the dark in rich medium and reaction centers were isolated (Paddock et al., 1989; Williams et al., 1992a). After isolation, the reaction centers were stored in 15 mM Tris-HCl, pH 8.0, 0.025% lauryldimethylamine *N*-oxide, and 1 mM EDTA buffer (TLE) at −75 °C. For all measurements, reaction centers referred to as wild type were those isolated from the ΔLM1.1 deletion strain containing a plasmid bearing the native *puf* operon.

Photosynthetic growth of the mutant strains was tested by inoculating liquid medium and solid agar with cells grown semiaerobically in the dark and then exposing the cultures to light under anaerobic conditions until they grew to stationary phase. Cell growth in liquid cultures was measured by monitoring the absorbance at 570 nm.

Steady-State Absorption Spectroscopy. Spectra of isolated reaction centers were measured using a Cary 5 spectrophotometer (Varian) at 295 and 20 K (Williams et al., 1992a). For the low-temperature measurements, glycerol was added to a final concentration of 33% (v/v) to isolated reaction centers in TLE, and the sample was cooled. Spectra were measured at a slew rate of 1 nm/s with a slit width of 2.5 nm from 1000 to 680 nm and with a slit width of 2.0 nm from 680 to 300 nm.

Time-Resolved Fluorescence Spectroscopy. Time-correlated single photon counting experiments were performed on a system described previously (Gust et al., 1990) using instrumental conditions and analysis outlined by Taguchi et al. (1992). Isolated reaction centers ($A_{802}^{1cm} \sim 1.5$) were prepared in 100 mM Tris-HCl, pH 8.0, 1 mM EDTA, and 0.05% Triton X-100 (Fluka). Immediately before the sample was added to a 0.15-cm cuvette, sodium dithionite (Fluka) was added to a final concentration of 5 mM to reduce the quinones. Fluorescence emission was measured utilizing a 10-ps, 4-MHz repetition rate pulse train at 860 nm for excitation and was detected at several wavelengths ranging from 880 to 940 nm at 295 K.

Data were fit using global analysis, with either three or four exponential components (Wendler & Holzwarth, 1987). Decay associated spectra were generated from the globally fit data and the resulting amplitudes were used to calculate the change in the standard free energy for the reaction $P^* \rightarrow P^+H_A^-$ for wild type and mutant reaction centers as described by Taguchi et al. (1992).

Time-Resolved Optical Absorption Spectroscopy. The rate of charge recombination from the state $P^+Q_A^-$ was measured at room temperature using the system described by Williams et al. (1992a). Isolated reaction centers ($A_{802}^{1cm} \sim 0.5$) were prepared in TLE. Prior to measurement, terbutryn was added to each sample to a final concentration of 0.5 mM terbutryn and 0.5% ethanol. The reaction centers were excited with a 10-μs pulse in the 300–600-nm spectral region from a xenon flash lamp, and changes in the absorbance at either 850 or 865 nm were recorded. The absorption decays were fit to a single exponential using a least-squares fit. Standard deviations were calculated from the average of several independent measurements.

The instrument and techniques used to measure the rates of the initial electron transfer were described by Taguchi et al. (1992). Isolated reaction centers ($A_{802}^{1cm} \sim 6$) were prepared in TLE in the presence of 0.5–1.0 mM terbutryn. Spectra were measured at 295 K with a dual diode array after excitation at 590 nm using a pulse width of ~200 fs. Light-induced changes in the absorption spectra from 830 to 960 nm with approximately 3-nm spectral resolution were recorded at 0.5-ps intervals between -5 and 45 ps after excitation. For measurement of the recovery of the absorption changes at 760 nm on longer time scales, the time dependence at 7-ps intervals of the absorbance changes at both 760 and 730 nm were simultaneously recorded and the two decay signals were subtracted.

For wild-type reaction centers, excitation power was adjusted to give a 10–15% bleaching of the ground-state Q_Y band of the dimer. This corresponds to approximately 10 μJ/pulse in a 2-mm-diameter spot. Similar pump powers were used for the FL(L167) mutant. For the HF(L168) mutant, the power was set at approximately half this level. At higher powers, the early time (0–500 fs) spectra exhibited additional, power-dependent features, particularly in the 800-nm region. Similar features can be seen in wild-type reaction centers when substantially higher powers (20–40 μJ/pulse) are used for excitation. The difference between the wild type and HF(L168) in this respect may represent different extinction coefficients for various Bchls at the excitation wavelength (590 nm).

Kinetic data were fit to a sum of exponential components. This was either done for a single trace, in the case of the 760–730-nm decay, or it was done globally using 70 wavelengths simultaneously at 2-nm intervals, and decay-associated spectra for each decay component were generated. For the analyses presented here, no deconvolution was performed.

Oxidation–Reduction Titrations. The P/P^+ midpoint potentials of purified reaction centers were determined by chemical redox titrations while monitoring both the ambient potential and the absorbance spectrum. Reaction centers were titrated in 100 mM Tris-HCl, pH 8.0, 1 mM EDTA, and 0.05% Triton X-100. Potassium hexacyanoferrate(III) (Fluka) and L-(+)-ascorbic acid, sodium salt (Fluka), were used as the oxidant and reductant, respectively. Titrants were made fresh daily at concentrations from 100 mM to 1 M in 10 mM Tris-HCl, pH 8.0, 1 mM EDTA, and 0.05% Triton X-100. For titrations, 10-mL reaction center samples (A_{802}^{1cm} = 0.2–0.6) were continuously stirred in a mixing chamber at 295 K. While mixing, the samples were flowed through a cuvette situated in the sample position of a double-beam Cary 5 spectrophotometer with a cuvette containing 10 mM Tris-HCl, pH 8.0, 1 mM EDTA, and 0.05% Triton X-100 in the reference position. A P101 platinum electrode (Radiometer) and K401 calomel reference electrode (Radiometer), attached to a Model 701A digital ion analyzer (Orion), were immersed in the sample and monitored the ambient potential. Prior to beginning the titration, the ambient potential of the sample was poised by the addition of potassium hexacyanoferrate(III) and sodium ascorbate to final concentrations of 100 and 50 μM, respectively. Each sample was titrated by increasing the ambient potential in 3–5-mV increments by adding small aliquots of potassium hexacyanoferrate(III). After each increase, both the ambient potential and the optical spectrum from 760 to 1000 nm were recorded. After the highest potential was reached, the spectra at decreasing potentials were measured after the addition of aliquots of sodium ascorbate. The absorption spectrum of fully oxidized reaction centers was determined by photooxidation of the dimer under saturating light conditions.

The potentiometer and electrodes were calibrated by comparing the measured potentials of equimolar solutions of potassium hexacyanoferrate(III) and potassium hexacyanoferrate(II) trihydrate made in four different buffers to the potentials determined by O'Reilly et al. (1973). This yielded a correction of 237 mV, which was used to convert values measured with the calomel reference electrode to the standard hydrogen electrode. A second calibration was performed by measuring potentials of saturated quinhydrone solutions (1:1 hydroquinone:benzoquinone, Sigma) prepared in several buffers poised at different pH values. The measured potentials, ranging from 200 to 400 mV, were plotted against calculated values, using a standard midpoint potential of 700 mV for quinhydrone (Bates, 1973). A least-squares fit of these data gave a correction of 238 mV, confirming the correction obtained using the hexacyanoferrate(III)/hexacyanoferrate(II) solutions.

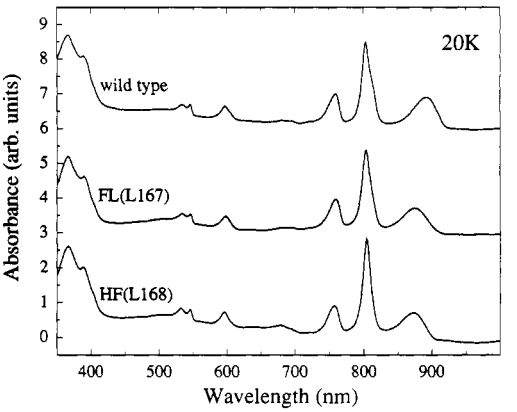

FIGURE 2: Steady-state, low-temperature (20 K) optical absorption spectra of wild-type and mutant reaction centers. The spectra are normalized at 760 nm. The 890-nm band and the shoulder to the red of the 800-nm band observed in the wild-type spectrum are shifted in the spectra of both mutants.

The extent of dimer reduction at each ambient potential was determined by monitoring the absorbance peak of the Q_Y band of the dimer, at 865 nm in wild type. To correct for intensity loss due to sample degradation, the measured absorbance at 865 nm was multiplied by the ratio of the initial absorbance at 800 nm to the measured absorbance at 800 nm. The slight blue shift and intensity increase of the 800-nm band, associated with dimer oxidation, introduces a small error in the normalization of the absorbance of the dimer peak but results in a difference of less than 5 mV in the calculated midpoint potential. The absorbance value at the dimer Q_Y band peak when the sample was photobleached (reaction centers should be 100% oxidized under these conditions) was subtracted to remove any background absorbance contributions. The corrected absorbance value for the dimer Q_Y band was then divided by the maximum absorbance value for the dimer Q_Y band, yielding the fraction of reaction centers reduced in the sample.

RESULTS

Bacterial Growth and Reaction Center Isolation. The mutants HF(L168) and FL(L167) containing the mutations L168 His to Phe and L167 Phe to Leu, respectively, were constructed. Reaction centers could be isolated from these mutants with an A_{280}/A_{800} ratio between 1.2 and 1.7. Reaction centers with an A_{280}/A_{800} ratio of $\sim$1.7 were used for most of the data acquisition. Both mutant strains grew photosynthetically in liquid and solid culture, but the HF(L168) mutant grew at approximately half the rate of the wild-type strain.

Optical Absorption Spectra. Room-temperature steady-state absorbance spectra of FL(L167) and HF(L168) reaction centers were similar to that of wild type except that the position of the Q_Y band of the dimer was shifted to 855 nm in FL(L167) and to 850 nm in HF(L168), compared to 865 nm in wild-type reaction centers (data not shown). In low-temperature (20 K) steady-state absorption spectra, the Q_Y band of the dimer was blue-shifted by approximately 20 nm in both FL(L167) and HF(L168) reaction centers relative to the wild-type band at 890 nm (Figure 2). The 800-nm band, which is attributed primarily to Bchl absorption, has a slight shoulder near 810 nm in the wild-type reaction center spectrum. This

Table I: Time-Resolved Fluorescence Decay Data[a]

strain	τ_1 (ps)	A_1	τ_2 (ps)	A_2	τ_3 (ps)	A_3	τ_4 (ps)	A_4	$P^*/P^+H_A^-$ ΔG^b (mV)
wild type	8.4	973	90.0	23.2	731	2.10	5120	1.41	−120
FL(L167)	15.3	964	119	30.3	894	3.90	5260	2.33	−115
HF(L168)[c]	15.2	982	164	16.0	1440	2.29			−140

[a] Values quoted above are from globally fit data. Excitation was at 860 nm and emission at 920 nm. Amplitudes have been normalized to sum to 1000. [b] The ratio of the prompt fluorescence amplitude (A_1) to the sum of the amplitudes of the remaining components ($A_2 + A_3 + A_4$) yields the equilibrium constant for $P^*/P^+H_A^-$. This ratio is corrected for the time resolution of the instrument using the measured P* decay time. The resulting equilibrium constant can be used to estimate a free energy gap between P* and $P^+H_A^-$ as described previously (Taguchi et al., 1992). The values are the average of several data sets; the estimated error is ±5 mV. [c] Only three components were needed to fit this data set.

feature is much less pronounced in the FL(L167) mutant and essentially absent in the HF(L168) mutant. The lack of this shoulder is not associated with any apparent loss of oscillator strength in the 800-nm spectral region, indicating that the 810-nm transition has shifted toward the dominant transition at 800 nm.

Time-Resolved Fluorescence Decay Measurements. The predominant decay of the fluorescence from quinone-reduced HF(L168) and FL(L167) reaction centers occurred with a time constant similar to that of the wild type, which is comparable to the time resolution of the apparatus (~10 ps). This fast fluorescence decay component was followed by low-amplitude fluorescence decay components on the 100-ps to nanosecond time scale. Fluorescence was measured at five wavelengths between 880 and 940 nm and the entire data set was analyzed globally using up to four exponential decay terms ($\sum_i A_i e^{-t/\tau_i}$). The initial amplitudes of the decay components (A_i) detected at 920 nm for wild type and both mutants are shown in Table I. In all cases the initial amplitudes of the long-lived components are much smaller than the initial amplitude of the prompt decay component, although the amplitudes of all the components of the decay in each sample had the same dependence on wavelength (data not shown). The long-lived fluorescence from wild-type reaction centers is thought to represent thermal repopulation of the excited singlet state of P after equilibration between the states P* and $P^+H_A^-$ on the picosecond time scale (Schenck et al., 1982; Woodbury & Parson, 1984). Changes in the relative amplitude of this fluorescence should thus be related to changes in the equilibrium constant for electron transfer from P to H_A. The relative amplitudes of the prompt and long-lived fluorescence components were similar in wild-type and FL(L167) reaction centers but the relative amplitudes of the long-lived components were much smaller in HF(L168) reaction centers (Table I). The longest, lowest amplitude component of the fluorescence that is observed in wild-type reaction centers was not detected in the HF(L168) decay analysis, indicating that thermal repopulation of P* was much more difficult in HF(L168) reaction centers, particularly at long times.

Charge Recombination Rate. The $P^+Q_A^-$ recombination rates for wild-type and mutant reaction centers were calculated from single-exponential fits of absorption changes monitored at 850 or 865 nm following excitation with a flash lamp (Table II). The recombination time slowed from 100 ms for wild-type reaction centers to 220 ms for HF(L168) reaction centers. FL(L167) reaction centers had a recombination time of 85 ms, slightly faster than that of wild-type reaction centers.

Initial Electron Transfer. Difference absorption spectra from 730 to 960 nm taken 0.5 and 33 ps after excitation with a 200-fs, 590-nm pulse are shown in Figure 3 for wild-type and HF(L168) reaction centers. The general features of the spectra from the wild type and the mutants are similar. The spectra of wild-type reaction centers have a large absorption

Table II: Summary of Electron Transfer Times and Dimer Midpoint Potentials

strain	$P^+Q_A^- \rightarrow PQ_A$ time[a] (ms)	P* decay time[a] (ps)	P/P^+ E_m[b] (mV)
wild type	100	3.8	495
FL(L167)	85	5.0	520
HF(L168)	220	3.6	415

[a] Estimated error is ±10%. [b] Estimated error in the midpoint potential is ±10 mV.

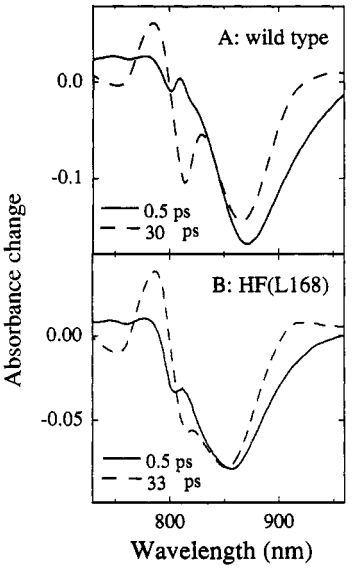

FIGURE 3: Difference absorption spectra measured for (A) wild-type reaction centers at 0.5 and 30 ps after excitation at 590 nm with a 200-fs pulse and (B) HF(L168) reaction centers at 0.5 and 33 ps after excitation. Magic-angle polarization between the excitation and probe pulses was used. Experimental parameters were as described in Taguchi et al. (1992).

decrease with a maximum at 870 nm that is primarily due to bleaching of the Q_Y band of the dimer (Figure 3A). This major bleaching is blue-shifted in both mutants and is centered at approximately 855 nm in the HF(L168) mutant (Figure 3B). The shift observed for this bleaching in the mutants is of a similar magnitude to the shifts of the ground-state Q_Y bands of the dimer at room temperature (data not shown). The early-time spectrum (0.5 ps) in wild type has a small bleaching near 800 nm that is probably due, at least in part, to excited states of B_A and B_B (Williams et al., 1992a). This bleaching is more pronounced in HF(L168) than in wild type.

Comparison of the time-resolved spectra reveals that the absorption changes in the 850–960-nm region have decreased between 0.5 and 33 ps (Figure 3). In wild type, these absorption changes have been attributed to stimulated emission from the excited singlet state of P (Woodbury et al., 1985; Martin et al., 1986; Chan et al., 1991). The stimulated emission from P* measured at 910 nm decays with a single-exponential lifetime of approximately 3.5 ps in wild-type

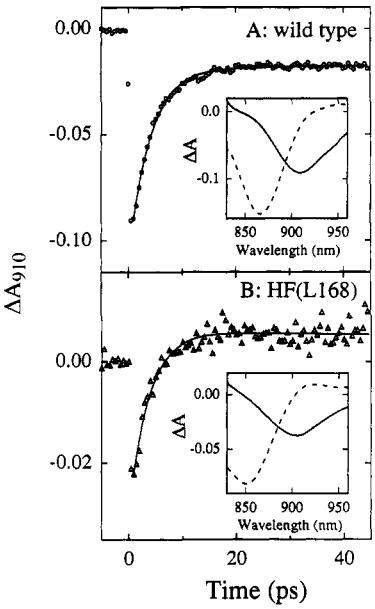

FIGURE 4: Kinetics of initial electron transfer in reaction centers. The decays of the stimulated emission of P* at 910 nm for (A) wild-type reaction centers and (B) HF(L168) reaction centers after photoexcitation at 590 nm with a 200-fs pulse are compared. The decays were fit globally to a single exponential and a constant term $[A(\lambda)e^{-kt} + B(\lambda)$, where λ is the wavelength] at 70 wavelengths covering this region of the spectrum. This yielded characteristic times of 3.8 and 3.6 ps for wild-type and HF(L168) reaction centers, respectively. Spectra of the resulting two amplitudes, $A(\lambda)$ (dashed line) and $B(\lambda)$ (solid line), are shown as insets.

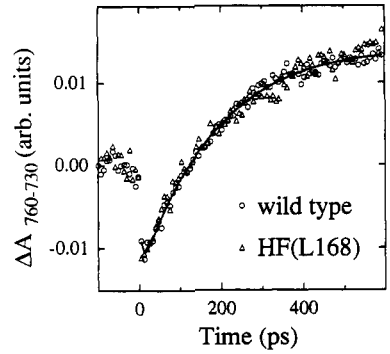

FIGURE 5: Kinetics of electron transfer from bacteriopheophytin to quinone. The recovery of the absorption changes at 760 nm in wild-type and HF(L168) reaction centers is shown. Dual-wavelength (760–730 nm) absorption changes were used to correct errors due to baseline drift. Least-squares fits of the data for wild type and HF(L168) yielded time constants of 200 and 220 ps, respectively. The fit for the wild-type data is depicted as a line.

reaction centers. A single-exponential fit of the decay of the stimulated emission at 910 nm results in a time of 4.5 ps for HF(L168) reaction centers, as previously reported (Williams et al., 1992b).

Fitting the absorbance changes at multiple wavelengths throughout this region of the spectrum results in a better statistical fit due to the larger data set used and also yields decay-associated spectra of the components (Figure 4). For wild type, this global analysis yielded a fast decay time of 3.8 ps and a constant term. The single-exponential lifetime of the stimulated emission obtained for the wild-type reaction centers is somewhat longer than some of the other values quoted in the literature (e.g., Martin et al., 1986; Holzapfel et al., 1990), due in part to the multiwavelength analysis employed. The time range of data collection also plays a significant role, as multiwavelength analysis of a wild-type data set taken over 20 ps, instead of 50 ps as in Figure 4, gave a 3.2-ps single-exponential decay time.

The insets to Figure 4 depict the wavelength dependence of the amplitudes of the two decay terms used in the fitting procedure, which assumes that the two decay times are wavelength-independent (Wendler & Holzwarth, 1987). The amplitude spectrum of the fast decay time has a minimum of about 910 nm, consistent with the assignment of this component to stimulated emission from P*. The amplitude spectrum of the constant term has a wavelength dependence very similar to that of the ground-state Q_Y band of P and presumably represents the bleaching of this band in the long-lived cation state of P. Decay times of 3.6 and 5.0 ps for the fast component of the global analysis were obtained for HF(L168) and FL(L167) reaction centers, respectively (Table II). Blue shifts in both the fast component and the constant term were observed in the amplitude spectra of the mutants relative to the wild type (Figure 4). The overall size of the difference absorption signal due to stimulated emission relative to that for the long-lived bleaching is about 30% smaller in HF(L168), but not in FL(L167), than it is in the wild type.

Fluorescence decay measurements on this time scale have suggested that the decay of P* may not be single-exponential (Du et al., 1992). When an additional exponential term was included in the multiwavelength analysis, the exponent lifetimes found were approximately 2.4 and 5.5 ps for wild-type reaction centers. This was accompanied by a slightly smaller error in the fit as measured by the least-squares deviation between the calculated and observed values. For HF(L168), increasing the number of components in the fit resulted in an additional long-lived, essentially constant, component and no significant improvement in the fit. All fits reported ignore the first 0.5 ps of data, since during this period excited states of the monomer Bchls due to 590-nm excitation contribute substantially to the transient absorption. Not including the initial 0.5 ps of data also made excitation pulse deconvolution and corrections for probe beam dispersion unnecessary.

No recovery of the bleaching of the Q_Y band of P at fast times was observed in the mutants. For example, no contribution of the Q_Y band of P is evident in the amplitude spectrum of the fast component (Figure 4) and the spectrum near 850 nm is unchanged between 0.5 and 33 ps (Figure 3) in HF(L168) reaction centers. This contrasts with a number of other mutants in the vicinity of the dimer, which show substantial ground-state recovery during the lifetime of P* (Kirmaier et al., 1988, 1989; Taguchi et al., 1992; Williams et al., 1992a). In accordance with previous work, the lack of ground-state recovery in the Q_Y band of P during the $P^* \rightarrow P^+H_A^-$ reaction is interpreted as an indication that the yield for electron transfer to H_A is essentially unity in the HF-(L168) and FL(L167) mutants.

Longer time-scale measurements were performed in the 760-nm region of the spectrum in order to determine the kinetics of electron transfer to Q_A. In wild-type reaction centers, the state formed within a few picoseconds is predominantly $P^+H_A^-$, resulting in a bleaching of the ground-state Q_Y transition of H_A at 760 nm. As the electron is transferred to Q_A, the bleaching at 760 nm recovers. The kinetics of absorption changes associated with the reoxidation of H_A are essentially identical in the wild type and the HF-(L168) mutant (Figure 5). Measurements on this time scale were not performed on the FL(L167) mutant.

P/P^+ Midpoint Potential. The oxidation–reduction midpoint potential of the electron donor was determined by performing chemical titrations of reaction centers. During

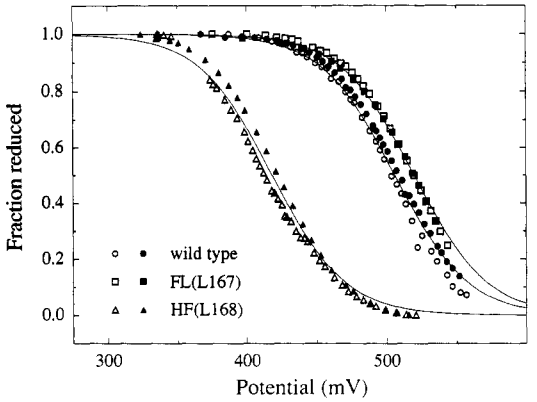

FIGURE 6: Oxidation–reduction titrations of wild-type and mutant reaction centers. The degree of reduction of P was followed by measuring the absorption of the P band (865 nm for wild type) while recording the ambient redox potential. The open symbols represent normalized data from oxidative titrations and the closed symbols represent data from reductive titrations performed on the same sample immediately after the oxidative titration. The solid lines represent fits of the Nernst equation ($n = 1$) to the combined data using one parameter, E_m, the midpoint potential. The midpoint potentials of FL(L167) and HF(L168) reaction centers are 25 mV higher and 80 mV lower than the wild-type value of 495 mV, respectively.

the titration, the ambient redox potential of the solution and the reaction center spectrum between 760 and 1000 nm were simultaneously monitored and the fraction of reduced reaction centers was calculated (Figure 6). The value of the midpoint potential, E_m, was obtained by fitting normalized data to the Nernst equation (Table II). Slightly better fits to the data could be obtained by adding additional parameters, such as adjusting for possible errors in the determination of the fraction of reactions centers that were reduced, but these corrections did not significantly alter the calculated values of the midpoint potentials. Each titration was performed in both the oxidative and reductive direction to ensure that the absorption changes observed were reversible. The slight hysteresis in the titration curve of HF(L168) may be partially due to poor equilibration of the ferri/ferrocyanide with the reaction centers in the potential range of this titration. The P/P^+ midpoint potential determined in this way for wild-type reaction centers was 495 ± 10 mV, in good agreement with the value reported by Moss et al. (1991). The P/P^+ midpoint potential determined for FL(L167) reaction centers was 25 mV above the wild-type value. In contrast, the midpoint potential of the dimer in HF(L168) reaction centers was decreased by 80 mV compared to wild-type reaction centers.

DISCUSSION

In order to test the concept that hydrogen-bonding interactions between the protein and the dimer are correlated with the redox properties of the dimer, a single-site mutation was constructed in which a histidine was exchanged for a phenylalanine at position 168 in the L subunit of the *Rb. sphaeroides* reaction center (Figure 1). His L168 is within hydrogen-bond distance of the acetyl group on ring I of the A side Bchl of the dimer (Yeates et al., 1988; El-Kabbani et al., 1991), and resonance Raman studies have suggested that a hydrogen bond exists between the protein matrix and this acetyl group (Robert & Lutz, 1986). Another mutation was made for comparison at the neighboring residue L167, exchanging phenylalanine for leucine (Figure 1). In both cases the residue was changed to the amino acid found at the symmetry-related position in the M subunit. Both the L167 Phe to Leu and L168 His to Phe mutations result in a change in the environment of the dimer, but the L168 His to Phe mutation results specifically in the loss of a hydrogen bond to the acetyl group of ring I.

The optical absorbance spectra of both the HF(L168) and FL(L167) mutant reaction centers showed blue shifts of 10–15 nm in the Q_Y absorption peak of the dimer. Shifts of this magnitude have been observed in reaction centers with other mutations near the dimer, such as L177 Ile to Asp and *syn1* (Williams et al., 1992a; Taguchi et al., 1992). While the size of these energy shifts (100–200 cm^{-1}) is consistent with calculated values for the effects of hydrogen bonding on the Q_Y transition energy of the dimer (Thompson et al., 1991), the blue shift cannot be exclusively correlated with changes in hydrogen bonding of the dimer. In low-temperature spectra, the HF(L168) mutant has a much less pronounced shoulder at ~810 nm than in the wild type. This is in contrast to other mutations made in the vicinity of the dimer that appear to shift the shoulder on the 800 nm band to longer wavelengths (Williams et al., 1992a). As has been suggested previously, these effects suggest some involvement of the dimer in transitions in this wavelength region, either directly or via coupling with the monomer Bchl transitions.

The redox potential of the electron donor is modified by specific interactions between the donor and the protein matrix. The L168 His to Phe mutation results in a decrease of 80 mV in the oxidation potential of the dimer. Several bacterial reaction center mutations have been reported previously in which an increase of at least 50 mV in the midpoint potential of the dimer has been postulated to result from the formation of a hydrogen bond between a histidine and ring I or ring V substituents of the dimer (Murchison et al., 1991; Stocker et al., 1992; Williams et al., 1992a). The addition of a hydrogen bond to the dimer is thus correlated with a substantial increase in the dimer midpoint potential, while the removal of a hydrogen bond results in an equally large decrease in the potential. A histidine forming a hydrogen bond with the dimer has a dipole directed from the partial negative charge of the nitrogen to the partial positive charge of the proton. The dipole is directed toward the carbonyl group of the Bchl and should destabilize the oxidized state of the donor. In agreement with the magnitude and direction of the effect observed in reaction centers, mutational studies of yeast cytochrome *c* has shown that the presence of a dipole oriented toward the heme results in a 55-mV increase in the redox potential of the heme (Langen et al., 1992).

Effects of the protein other than hydrogen bonding could contribute to the changes in the midpoint potential of the dimer observed in the mutants. The removal of the histidine in the HF(L168) mutant could cause a rotation of the acetyl group of ring I that would cause changes in the electronic energy levels of the dimer (Lendzian et al., 1990). However, changes of similar magnitude in the dimer midpoint potential are observed for the mutations near the ring V keto carbonyl (Williams et al., 1992a). These mutations should not cause structural alterations of the Bchls, indicating that changes in hydrogen bonding are sufficient to shift the redox potential significantly. The oxidized state of the electron donor should also be stabilized by more general electrostatic interactions between the donor and surrounding polar residues. In the FL(L167) mutation, a residue near the donor is replaced with a more hydrophobic residue, resulting in an increase of 25 mV in the dimer midpoint potential. This increase in potential is consistent with the correlation between an increase in the redox potential and a decrease in solvent exposure observed in comparative studies of different cytochromes [reviewed in

Moore and Pettigrew (1990)] and different mutants of cytochrome *c* (Louie et al., 1988).

The driving force for the initial electron transfer is the energy difference between P* and the initial charge-separated state. The driving force should increase as the oxidation potential of the dimer decreases. For both the HF(L168) and FL(L167) mutants, the ~15-nm blue shift of the Q_Y band of P corresponds to a 25-meV increase in the driving force due to the increase in the P/P* energy difference. For the FL(L167) mutant, this increase in the driving force is offset by the 25-mV increase in the P/P^+ midpoint potential. In the HF(L168) mutant, both the 80-mV decrease in the P/P^+ midpoint potential and the 25-meV increase in the P/P* energy difference should increase the driving force for the initial electron transfer.

Although there is no simple way to measure the $P^+B_A^-$ free energy, the standard free energy difference between P^*H_A and $P^+H_A^-$ can be estimated by measuring fluorescence due to the residual P* which remains after P* and $P^+H_A^-$ have come to equilibrium. The results of these experiments show a significant decrease in the level of long-lived fluorescence in the HF(L168) mutant (Table I), indicating an increase in the equilibrium constant favoring the forward reaction and therefore an increase in the energy gap between P* and $P^+H_A^-$. An equilibrium model was used to calculate the $P^*/P^+H_A^-$ free energy difference (Table I), as has been done previously for the wild type and other mutants (Woodbury & Parson, 1984; Taguchi et al., 1992; Williams et al., 1992a). The calculated free energy difference was determined to be unchanged for the FL(L167) mutant, in agreement with the other measurements. However, only a 20-mV increase in the free energy difference was calculated for the HF(L168) mutant, in contrast to the ~100-mV increase indicated by the redox and spectral measurements. Of the three long-lived fluorescence decay components used in the calculation of the $P^*/P^+H_A^-$ free energy difference, the longest lived component of the delayed fluorescence has been most convincingly associated with $P^+H_A^-$ decay (e.g., Woodbury & Parson, 1984). In the HF(L168) mutant, the longest-lived component is not evident in fluorescence from quinone-reduced reaction centers (Table I). Although the loss of this state may indicate a much shorter lifetime of $P^+H_A^-$ in the mutant compared to wild type, it is more likely that the fluorescence due to equilibration between P* and $P^+H_A^-$ on the nanosecond time scale is dramatically diminished (at least by a factor of 10), consistent with the conclusion that the free energy gap between P* and $P^+H_A^-$ is much larger in HF(L168) than in wild-type reaction centers. The remaining fluorescence in the 100 ps to 1.4 ns time range has a spectrum consistent with P*, however it may represent something other than an equilibration between P* and $P^+H_A^-$, such as P* decay in a small population of reaction centers that do not undergo electron transfer with fast rates. Such background fluorescence that is not sensitive to the redox potential of P may explain in part the apparent insensitivity of the $P^*/P^+H_A^-$ free energy gap to large increases in the P/P^+ midpoint potential in other mutants (Williams et al., 1992a; Taguchi et al., 1992; Stocker et al, 1992).

The rate of the initial electron transfer in the HF(L168) mutant essentially does not change compared to wild type despite a large decrease in the P/P^+ midpoint potential. However, in mutants in which the P/P^+ midpoint potential increases, a decrease in the initial electron transfer rate is observed (Williams et al., 1992a). A correlation between the free energy difference and the initial electron transfer rate in reaction centers is complicated by uncertainty concerning the role of B_A in this reaction. The state $P^+B_A^-$ may act as a populated intermediate for electron transfer or as a virtual state mediating transfer between P and H_A (Holzapfel et al., 1990; Kirmaier & Holten, 1991). If $P^+B_A^-$ is a populated state whose energy is below that of P*, then the decrease in the P/P^+ midpoint potential in the HF(L168) mutant should increase the $P^*/P^+B_A^-$ free energy difference, which would be the driving force for the initial electron transfer. The observed weak dependence of the initial rate on driving force for free energy differences that are larger than wild type implies that higher vibrational modes may be important for electron transfer between P* and $P^+B_A^-$ [see, for example, Alden et al. (1992)]. If $P^+B_A^-$ serves as a virtual state which couples P* and $P^+H_A^-$, both the electronic coupling between P* and $P^+H_A^-$ and the free energy gap for the overall reaction are changed in the mutant. Using this superexchange model, the energy of the $P^+B_A^-$ virtual state has been estimated to lie at most 100 meV above that of P* (Marcus, 1988; Du et al., 1992). Thus, the decrease in the P/P^+ midpoint potential in the HF(L168) mutant would result in lowering the $P^+B_A^-$ energy to a level close to or below that of P*. If $P^+B_A^-$ remains above or near P* in the HF(L168) mutant, a decrease in the $P^*/P^+B_A^-$ energy difference of this magnitude should result in a significant increase in the rate of the initial electron transfer. Alternatively, if $P^+B_A^-$ drops substantially below P* in this mutant, the $P^+B_A^-$ state should become populated and a significant change in the spectral signature of intermediate states in the transient absorption spectra would be expected. Models utilizing a superexchange mechanism need to accommodate the lack of any large changes in either the rate or the spectra in the HF(L168) mutant.

Changes in the initial electron transfer rate may result from effects other than shifts in the free energy difference between P* and the initial charge separated state. This places limits on the quantitative interpretation of the correlations observed in the hydrogen-bond mutants. For example, the electron transfer time in the FL(L167) mutant increases to 5.0 from 3.8 ps in the wild type, despite a driving force that is similar to the wild type.

The P/P^+ midpoint potential should be proportional to the driving force for the $P^+Q_A^- \rightarrow PQ_A$ charge recombination reaction. In contrast to the initial electron transfer, the charge recombination rate is not optimized in the wild type. A faster rate is observed in the FL(L167) mutant, which has a higher midpoint potential and thus a larger driving force, and a slower rate is observed in the HF(L168) mutant, which has a lower midpoint potential and therefore a smaller driving force. The correlation of the midpoint potential with the charge recombination rate can be modeled and is in agreement with other measurements (Williams et al., 1992b).

In summary, mutations that potentially alter hydrogen bonding between amino acid residues and ring I or ring V substituents of the Bchl dimer are correlated with changes in the redox potential of the dimer as well as the driving force for electron transfer and charge recombination. These mutants provide a system for studying the effects of redox potential on electron transfer processes since they result in changes of the dimer midpoint potential over a large range in both directions. Measurements of the kinetics and thermodynamics of electron transfer as a function of temperature are in progress as well as detailed spectral measurements of the intermediate states involved in the initial electron transfer.

ACKNOWLEDGMENT

We wish to thank V. H. Coryell and X. Zhang for their assistance with preparation of reaction centers.

REFERENCES

Alden, R. G., Cheng, W. D., & Lin, S. H. (1992) *Chem. Phys. Lett. 194*, 318–326.

Allen, J. P., Feher, G., Yeates, T. O.; Komiya, H., & Rees, D. C. (1987) *Proc. Natl. Acad. Sci. U.S.A. 84*, 5730–5734.

Bates, R. G. (1973) *Determination of pH, Theory and Practice*, John Wiley & Sons, New York.

Chan, C.-K., Chen, L. X., DiMagno, T. J., Hanson, D. K., Nance, S. L., Schiffer, M., Norris, J. R., & Fleming, G. R. (1991) *Chem. Phys. Lett. 176*, 366–372.

Du, M., Rosenthal, S. J., Xie, X., DiMagno, T. J., Schmidt, M., Hanson, D. K., Schiffer, M., Norris, J. R., & Fleming, G. R. (1992) *Proc. Natl. Acad. Sci. U.S.A. 89*, 8517–8521.

El-Kabbani, O., Chang, C.-H., Tiede, D., Norris, J., & Schiffer, M. (1991) *Biochemistry 30*, 5361–5369.

Feher, G., Allen, J. P., Okamura, M. Y., & Rees, D. C. (1989) *Nature 339*, 111–116.

Gust, D., Moore, T. A., Luttrull, D. K., Seely, G. R., Bittersmann, E., Bensasson, R. V., Rougée, M., Land, E. J., De Schryver, F. C., & Van der Auweraer, M. (1990) *Photochem. Photobiol. 51*, 419–426.

Holzapfel, W., Finkele, U., Kaiser, W., Oesterhelt, D., Scheer, H., Stilz, H. U., & Zinth, W. (1990) *Proc. Natl. Acad. Sci. U.S.A. 87*, 5168–5172.

Kirmaier, C., & Holten, D. (1987) *Photosynth. Res. 13*, 225–260.

Kirmaier, C., & Holten, D. (1991) *Biochemistry 30*, 609–613.

Kirmaier, C., Holten, D., Bylina, E. J., & Youvan, D. C. (1988) *Proc. Natl. Acad. Sci. U.S.A. 85*, 7562–7566.

Kirmaier, C., Bylina, E. J., Youvan, D. C., & Holten, D. (1989) *Chem. Phys. Lett. 159*, 251–257.

Langen, R., Brayer, G. D., Berghuis, A. M., McLendon, G., Sherman, F., & Warshel, A. (1992) *J. Mol. Biol. 224*, 589–600.

Lenzian, F., Endeward, B., Plato, M., Bumann, D., Lubitz, W., & Möbius, K. (1990) in *Reaction Centers of Photosynthetic Bacteria* (Michel-Beyerle, M. E., Ed.) pp 57–68, Springer-Verlag, Berlin.

Louie, G. V., Hutcheon, W. L. B., & Brayer, G. D. (1988) *J. Mol. Biol. 199*, 295–314.

Marcus, R. A. (1988) in *The Photosynthetic Bacterial Reaction Center: Structure and Dynamics*, (Breton, J., & Verméglio, A., Eds.) pp 389–398, Plenum, New York.

Martin, J.-L., Breton, J., Hoff, A. J., Migus, A., & Antonetti, A. (1986) *Proc. Natl. Acad. Sci. U.S.A. 83*, 957–961.

Michel, H., Epp, O., & Deisenhofer, J. (1986) *EMBO J. 5*, 2445–2451.

Moore, G. R., & Pettigrew, G. W. (1990) *Cytochromes c*, Springer-Verlag, Berlin.

Moss, D. A., Leonhard, M., Bauscher, M., & Mäntele, W. (1991) *FEBS Lett. 283*, 33–36.

Murchison, H. A., Woodbury, N. W., Taguchi, A. K., Allen, J. P., & Williams, J. C. (1991) *Biophys. J. 59*, 182a.

O'Reilly, J. E. (1973) *Biochim. Biophys. Acta 292*, 509–515.

Paddock, M. L., Rongey, S. H., Feher, G., & Okamura, M. Y. (1989) *Proc. Natl. Acad. Sci. U.S.A. 86*, 6602–6606.

Robert, B., & Lutz, M. (1986) *Biochemistry 25*, 2303–2309.

Scheer, H., Ed. (1991) *Chlorophylls*, CRC Press, Boca Raton, FL.

Schenck, C. C., Blankenship, R. E., & Parson, W. W. (1982) *Biochim. Biophys. Acta 680*, 44–59.

Simon, R., Priefer, U., & Pühler, A. (1983) *Bio Technology 1*, 784–791.

Stocker, J. W., Taguchi, A. K. W., Murchison, H. A., Woodbury, N. W., & Boxer, S. G. (1992) *Biochemistry 31*, 10356–10362.

Taguchi, A. K. W., Stocker, J. W., Alden, R. G., Causgrove, T. P., Peloquin, J. M., Boxer, S. G., & Woodbury, N. W. (1992) *Biochemistry 31*, 10345–10355.

Thompson, M. A., Zerner, M. C., & Fajer, J. (1991) *J. Phys. Chem. 95*, 5693–5700.

Wendler, J., & Holzwarth, A. R. (1987) *Biophys. J. 52*, 717–728.

Williams, J. C., Alden, R. G., Murchison, H. A., Peloquin, J. M., Woodbury, N. W., & Allen, J. P. (1992a) *Biochemistry 31*, 11029–11037.

Williams, J. C., Woodbury, N. W., Taguchi, A. K. W., Peloquin, J. M., Murchison, H. A., Alden, R. G., & Allen, J. P. (1992b) in *The Photosynthetic Bacterial Reaction Center II: Structure, Spectroscopy, & Dynamics* (Breton, J., & Verméglio, A., Eds.) pp 25–31, Plenum, New York.

Woodbury, N. W. T., & Parson, W. W. (1984) *Biochim. Biophys. Acta 767*, 345–361.

Woodbury, N. W., Becker, M., Middendorf, D., & Parson, W. W. (1985) *Biochemistry 24*, 7516–7521.

Woodbury, N. W., Taguchi, A. K., Stocker, J. W., & Boxer, S. G. (1990) in *Reaction Centers of Photosynthetic Bacteria* (Michel-Beyerle, M. E., Ed.) pp 303–312, Springer-Verlag, Berlin.

Yeates, T. O., Komiya, H., Chirino, A., Rees, D. C., Allen, J. P., & Feher, G. (1988) *Proc. Natl. Acad. Sci. U.S.A. 85*, 7993–7997.